RSC Advances

PAPER

View Article Online
View Journal | View Issue

Cite this: *RSC Adv.*, 2022, **12**, 29375

Theoretical prediction and design for chalcogenide-quantum-dot/TiO_2 heterojunctions for solar cell applications†

Kangqi Shen, *[a] Govindarajan Saranya [a] and Mingyang Chen *[ab]

Received 17th August 2022
Accepted 7th October 2022

DOI: 10.1039/d2ra05116h

rsc.li/rsc-advances

Quantum dot sensitized solar cells have attracted much attention due to their high efficiency of photoelectric conversion and low manufacturing cost. In this study, a series of heterojunction structures with cubic $(MA)_4$ chalcogenide quantum dots adsorbing on the (001) surface of TiO_2 were investigated, in order to explore new quantum dot sensitizers for solar cell applications. Our study revealed that sulfide and selenide quantum dots are more suitable for solar energy harvesting, compared to their oxide counterparts, due to their smaller ionization potentials and smaller HOMO–LUMO (highest occupied molecular orbital-lowest unoccupied molecular orbital) gaps, but in general exhibit weaker adsorption on TiO_2. M_4A_3B and $M_4A_2B_2$ quantum dots were designed in combination with the advantage of higher adsorption stability and photoelectric conversion capability. Our theoretical predictions for the structurally precise chalcogenide systems suggest a possible direction for the design of quantum-dot sensitized solar cells.

1. Introduction

With the continuous development of human society, the non-renewable fossil energy with a negative impact on the environment will eventually be replaced by environment-friendly renewable energy. Searching for renewable alternative energy solutions is eminently important, which inspires rapidly growing interest and a wide range of research fields. Among the possible solutions for fossil energy replacement, solar energy is regarded as a suitable energy source due to its sustainability and environment friendliness. To utilize the solar energy, designing and manufacturing low-cost high-stability solar cells with high power conversion efficiency (PCE) is a key area of study. Since the production of the first doped silicon semiconductor solar cells at Bell Laboratory in the United States in 1954, semiconductor solar cell research is in the ascendant.[1] In 1961, William Shockley and Hans Queisser gave a theoretical photovoltaic conversion efficiency of 30% for silicon solar cells, known as the Shockley–Queisser Limit, and the photovoltaic efficiency of modern semiconductor solar cells is 33.7% in the theory of arbitrary single-junction cells.[2,3] For the purpose of lower manufacturing cost and better photoelectric conversion efficiency, the quantum dot sensitized solar cells (QDSSC) with the properties of variable absorption spectrum caused by multi-electron excitation (MEG) and quantum confinement effect are considered as ideal photoelectric systems for the next generation,[4–6] with a maximal theoretical power conversion efficiency of 42%.[7]

The QDSSC is a successor to dye-sensitized solar cells (DSSCs) which were first proposed by O'Regan and Gratzel in 1991. This spurred the field of sensitized solar cells and essentially paved the way for the recent 20 years of research in this field.[8–11] Currently, the search for stable non-toxic organic dyes that cover the whole solar spectrum as a sensitizer remains challenging; for example, the widely used ruthenium complexes have high photoelectric conversion characteristics but suffer from their high production costs and poor long-term stability.[12] Therefore, using narrow bandgap semiconductor quantum dots, such as CdS or CdSe as alternatives to organic dyes, to sensitize the wide-bandgap anode materials, such as TiO_2, is promising and has become a new direction for sensitized solar cells.[13,14] Nozik's group successfully published groundbreaking research on quantum dot sensitized solar cells in 2001.[15] With research in recent years, the photoelectric conversion efficiency of quantum dot sensitized solar cells increased from less than 5% in 2010 to 12.98% in 2019.[16–18]

The structure of QDSSCs can be divided into the following parts: mesoporous semiconductor thin films, quantum dot sensitizers, electrolytes and counter electrodes. After describing the composition of quantum dot sensitized solar cells, the working principle is further explained below. First, quantum dots adsorbed on the surface of oxide semiconductor films

[a]*Beijing Computational Science Research Center, Beijing 100193, China. E-mail: shenkangqi@csrc.ac.cn*

[b]*Center for Green Innovation, School of Materials Science and Engineering, University of Science and Technology Beijing, Beijing 100083, China. E-mail: Chinamychen@ustb.edu.cn*

† Electronic supplementary information (ESI) available. See DOI: https://doi.org/10.1039/d2ra05116h

absorb sunlight and generate photoelectron–hole pairs. Photoelectrons are then rapidly injected into the conduction band of wideband gap metal oxide. The photogenerated electrons injected into the metal oxide conduction band are transferred to the conductive substrate and arrive at the counter electrode *via* an external circuit. At the same time, the holes left the quantum dot valence band and oxidized the redox couple in the electrolyte to the oxidation state. The oxidized redox couple then diffuses to the counter electrode and is reduced by the electrons transported through the external circuit. All of these constitute the entire circuit, and photocurrent is generated in the external circuit.

The sensitizing of the wide-bandgap semiconductor is key to developing efficient QDSSCs. The heterojunction between the QD and the wide band-gap semiconductor is one of the most important design factors for QDSSC. Quantum dots (QDs) are a kind of quasi-zero-dimensional nanomaterial, which generally refers to nanocrystals with sizes within tens of nano meters in three dimensions. The wavelength of light absorption of quantum dots varies with their size (the smaller the quantum dots, the shorter the wavelength of light absorption), so the size of quantum dots can realize the regulation of the wavelength length of light absorption, and can absorb light in a wide wavelength range.[7,19] This is called the quantum size effect. Another feature, multi-electron excitation of QDSSC also can improve the photoelectric conversion properties in theory. This effect allows greater utilization of solar energy in low wavelength segments, and would allow quantum dot solar cells to exceed the Shockley–Queisser limit of single-excited solar cells, achieving about 42% theoretical photoelectric conversion efficiency (PCE).[20–22]

Titanium dioxide (TiO_2) is a cheap and non-toxic material with good chemical stability, good photocatalytic activity, and larger specific surface area, and thus is commonly adopted as the solar cell light anode film base material. As a wide-bandgap semiconductor (rutile 3.0 eV, anatase 3.2 eV), TiO_2 majorly absorbs ultraviolet light, which accounts for only ~4% of the solar energy, and therefore, TiO_2 needs to be sensitized in order to achieve higher photoelectric conversion efficiency.[23] TiO_2-based photoanodes have been widely used in DSSCs and QDSSCs, and are relevant in QDSSC applications with record-high conversion efficiencies so far. Titanium dioxide is also widely used in photocatalysis to split water to make hydrogen or oxygen or reduce carbon dioxide.[24,25]

As a panchromatic sensitizer, quantum dots make up for the narrow absorption range and low absorption coefficient of conventional sensitizers. The ideal quantum dot sensitizer should meet two conditions, the first being that the band gap is appropriate, the second that the light absorption coefficient is good, and can effectively absorb sunlight, to achieve the outstanding enhancement of PCE. In addition, the matching degree of energy levels is also a major factor affecting the photoelectric performance, and the conduction band bottom of the quantum dot sensitizer material is generally higher than that of the adsorbed semiconductor oxide material (such as TiO_2, WO_3, SnO_2). Currently, commonly used mononuclear quantum dots include CdS, CdSe, PbS, *etc.*[26–28] However, mononuclear quantum dots usually have the limitation that the performance of the sensitizer cannot be taken into account. In the process of optimizing and exploring new sensitizers, the realization of cosensitization effects of various quantum dots, the excavation and exploration of binary quantum dots with narrower band gap, and even the successful synthesis and application of multicomponent alloy quantum dots have all been studied in depth to varying degrees. For example, Zhang *et al.* optimized the aperture of TiO_2 photoanodes and made the efficiency of CdS/Cdse QDSSCs reach 4.92%.[29] Du *et al.* adopted ZnCuInSe quantum dots synthesized by an organic high-temperature thermal injection method with absorption edge up to 1000 nm. They achieved a breakthrough improvement in photocurrent and finally achieved an excellent photoelectric conversion efficiency (11.61%).[30] In 2017, Zhong's group presented a new type of solar cell with TiO_2 as base and ZClSe as quantum dots, achieving a PCE of ~13%.[31]

CdS and CdSe QDs are the most mature in applications in QDSSCs, mainly because the energy level positions of CdS and CdSe QDs can match well with TiO_2 and maintain good physical and chemical stability in electrolytes. Meanwhile, their preparation process is very simple, so they have been widely used. Because CdS has a wide band gap (2.4 eV) and a high conduction band, it has the disadvantage of a narrow light absorption range. CdSe has a wide absorption range up to 700 nm, but its conduction band position is relatively low, resulting in a lower electron injection rate. So we tried to find various related chalcogenide-quantum-dots to improve on these shortcomings.

Recent advances in the synthesis and morphological control of nanoclusters and quantum dots make it possible to design and control quantum dots at the atomic level.[32–34] At the same time, improved experimental methods can deposit quantum dots on semiconductor thin films better.[35,36] With the ascension of computer performance, first principles calculation of hundreds of atoms can be used to explore the photo-anode characteristics of QDSSC. Chen *et al.* predicted that small rocksalt nanoclusters such as MgO, CaO, and CdO have smaller optical gaps than nanoparticles and clusters and the gaps are tunable with particle size.[37,38] The surface adsorbed small QDs are expected to be electronically and optically different to the gap-phase forms, as part of the electronic structure of the QD will be assimilated by the wide-bandgap semiconductor upon the surface adsorption with strong ionic bonds. Consequently, small metal oxide clusters that will exhibit visible absorption in the gas phase exhibit a larger optical gap on a substrate and become unsuitable for solar applications. Meanwhile, sulfides and selenides that commonly exhibit lower work functions and smaller optical gaps than oxides may exhibit suitable solar harvesting capability in the heterojunction. It will be interesting to see the electronic and optical properties of the heterojunction between the small chalcogenide rocksalt QDs and a wide-bandgap semiconductor, and find out whether they are suitable for QDSSCs.

In this study, we explore a class of new QDSSCs with structurally precise cubic $(MA)_4$ QDs as the sensitizers and TiO_2 as the wide-bandgap semiconductor. First, a set of quantum dots

of sulfides (CdS, AsS, ZnS, GeS, SnS and InS), oxides (CdO, BeO, MgO, CaO, SrO and BaO) and selenide (CdSe) were designed. From the adsorption stability, light absorption intensity and effective photoexcitation intensity of QDSSC, sulfides and selenide have better light absorption and conversion properties than oxides, but their adsorption stability is not as good as oxides. Then a series of heterojunction structures with cubic M_4A_3B and $M_4A_2B_2$ chalcogenide quantum dots adsorbing on the (001) surface of TiO_2 were designed. To do this, we predict their geometric structure, binding energy, electronic structure, and optical properties. It was found that the adsorption stability of the M_4A_3B and $M_4A_2B_2$ chalcogenide quantum dots was greatly improved, and the light absorption performance was slightly decreased, while the photoelectric conversion efficiency was basically unchanged.

2. Computation method

To build the QD/TiO_2 heterojunction, cubic $(MA)_4$ QDs (M = Cd, Be, Mg, Ca, Sr, Ba, Zn, Ge, As, In and Sn; A = O, S, and Se), cubic M_4A_3B and $M_4A_2B_2$ QDs (M = Cd, As and In; A = S and Se; B=O) in a $2 \times 2 \times 2$ lattice, were chosen and placed on a TiO_2 anatase (001) surface slab. The TiO_2 anatase (001) surface slab is constructed from a $4 \times 2 \times 2$ crystal cut with a total number of 64 TiO_2 units and a size of $15.10 \times 15.10 \times 30.91$ Å^3. A vacuum of 20 Å were placed between the TiO_2 slab and its periodic mirror images along the *c* direction. All of the geometry optimization calculations, electronic structure calculations, and light absorption calculations were calculated by Vienna *ab initio* simulation package (VASP).[39] Perdew–Burke–Ernzerhof (PBE) exchange-correlation functional and the projected augmented wave (PAW) potentials have been used in above calculation.[40,41] The electronic wavefunctions were expanded using planewaves with cutoff energy of 600 eV. The energy and force were set to converged to 10^{-4} eV and 0.1 eV Å^{-1}. The Brillouin zone was sampled using a $4 \times 4 \times 4$ Monkhorst–Pack grid for the bulk, and $4 \times 4 \times 1$ Monkhorst-Pack grid for the calculations of the QD/TiO_2 systems.[42]

3. Results and discussion

3.1 Geometry

As the photoanode of quantum dot sensitized battery, the stability of QD/TiO_2 composite structure is very important. Let's observe the geometry of different quantum dots on the surface of TiO_2(001) in QD/TiO_2(001) system, as shown in Fig. 1 and S1.† There are about three geometry types, the typical structure of first type is the In_4S_4/TiO_2(001) composite system (Fig. 1a), which shows S of In_4S_4 is facing Ti of TiO_2 surface. In of In_4S_4 is directly facing the midpoints of each side of the square on the surface of TiO_2(001), and both side points are occupied by O of TiO_2. It can be seen that such cube quantum dots are fitted onto the surface of TiO_2 in a very regular way. This kind of geometry could been seen in some $(MA)_4/TiO_2$(001) systems, such QD as Mg_4O_4, Ca_4O_4, Cd_4O_4, Cd_4S_4, Sn_4S_4, Ge_4S_4 (Fig. S1†). The second type are geometrically deformed by this configuration, which can be seen in Fig. 2b. There is still a fully structured quantum dot in As_4S_4/TiO_2(001) adsorption system, but it is no longer a cube, and it is

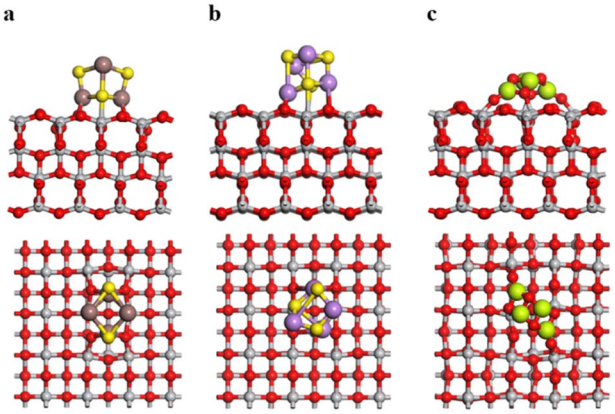

Fig. 1 The geometry of the optimized adsorption system (a) In_4S_4/TiO_2(001), (b) As_4S_4/TiO_2(001), (c) Be_4O_4/TiO_2(001).

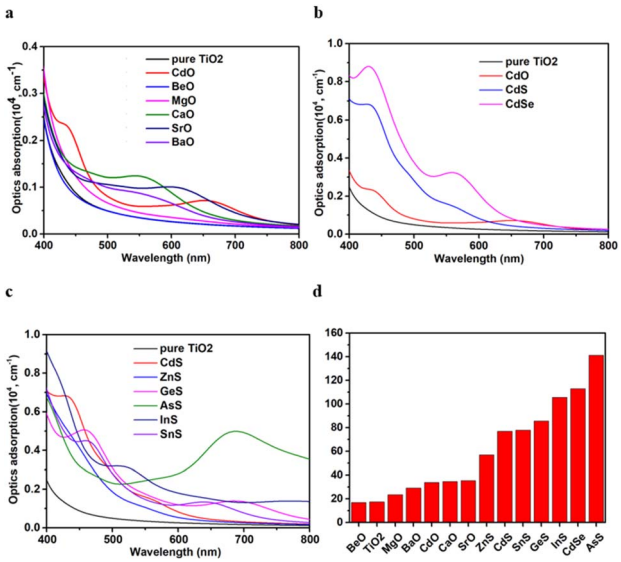

Fig. 2 $(MA)_4/TiO_2$(001) optical absorption: (a) oxide quantum dot/TiO_2(001) optical absorption spectrum, (b) Cd – containing compound quantum dot/TiO_2(001) optical absorption spectrum, (c) sulfide quantum dot/TiO_2(001) optical absorption spectrum, (d) the integral area of each light absorption spectrum in the visible band of 400–800 nm.

tilted rather than flat on the TiO_2 with one As of As_4S_4 closer to the surface. While in Cd_4Se_4/TiO_2(001) adsorption system, the distortion of quantum dots is intensified and adsorbs on TiO_2 more obliquely. There's another geometry like Zn_4S_4/TiO_2(001) adsorption system, quantum dot did not deform significantly, just changed from a flat cube to a tilted one. Finally, there are several adsorption systems in which the original structure of the quantum dots has been completely torn apart, like Be_4O_4/TiO_2(001), Sr_4O_4/TiO_2(001), Ba_4O_4/TiO_2(001) in Fig. S1.†

3.2 Optical absorption

The optical absorption and conversion efficiency of the photoanode of QDSSCs are important indexes which affect its performance. The predicted absorption spectra for the $(MA)_4$

chalcogenide-QD/TiO_2 heterojunction are shown in Fig. 2. From Fig. 2a, it can be intuitively seen that the optical absorption effect of the system after quantum dot sensitization is better than that of the pure TiO_2 film surface, and the optical absorption enhancement amplitude of all oxide quantum dot systems is low in value. The intensity of light absorption of quantum dot adsorption system is highly correlated with the bonding element, as shown in figure Fig. 2b, the light absorption of Cd_4Se_4/TiO_2 (001) adsorption system from blue to red light gradually decline, is always the highest, Cd_4S_4/TiO_2 (001)'s adsorption is the second near the blue light, while the absorption ability of Cd_4O_4 as oxide in this section is bad, and it's performance of near-red band after 600 nm only slightly improves than Cd_4S_4, which is similar to Cd_4Se_4. In Fig. 2c, the light absorption intensity of the photoanode of all sulfide quantum dot sensitized solar cells is greatly improved. The most intuitive one is that As_4S_4/TiO_2(001) abnormally increases the light absorption at 600–800 nm by a large amount, while other adsorption systems are at a relatively low level in this light band. After having a visual understanding of the light absorption spectra of different QD/TiO_2 adsorption systems, we need introduce a more quantitative index to analyze the light absorption intensity of each adsorption system. According to the area of each light absorption spectral line in the visible spectrum of 400–800 nm in these figures, the light absorption results of each adsorption system can be intuitively compared (Fig. 2d). Consistent with our intuitive impression, the As_4S_4/TiO_2(001) adsorption system has the largest integrated area of light absorption from 400 nm to 800 nm, thanks to its high absorption intensity throughout the light band and outstanding absorption peak between 600 and 800 nm. The Cd_4Se_4/TiO_2 (001) adsorption system ranks the second in the light absorption score table, with a high absorption peak between 400 and 450 nm and a small absorption peak between 550 and 600 nm. Then the light absorption spectral line decreases rapidly after 600 nm, that is, the absorption near the red light is not good. Next, In_4S_4/TiO_2 (001) adsorption system was found to be ranked third in the light absorption integral area table, Its entire absorption spectrum shows a gentle decline from 400 to 800 nm, and the light absorption declines more slowly at the band of 600 to 800 nm, and maintains a higher absorption intensity than other adsorption systems except As_4S_4/TiO_2(001). The above three adsorption systems can be regarded as the first echelon of light absorption, The remaining sulfide quantum dot adsorption systems, including Ge_4S_4, Sn_4S_4, Cd_4S_4, and Zn_4S_4, can be considered the second tier. In the third tier, all the worst light absorption systems are oxide quantum dot adsorption systems, which reveals the adverse effects of oxygen elements on light absorption. For quantum dot sensitized solar cells, the photo absorption performance of photoanode can be regarded as the first key factor affecting its PCE. In this test, oxides generally perform poorly, while sulfides and selenides show relatively excellent light absorption performance.

3.3 Electronic structure and effective photoexcitation intensity

The electron state of the photoanode composite system reflects how many electrons can be transferred from the excited state of quantum dots to the conduction band of the substrate material. Therefore, the partial density of states (PDOS) of the QD/TiO_2(001) composite system should be provided to assist the judgment (Fig. 3). In order to display the electron transfer performance of each adsorption system more clearly, the key information in PDOS is also summarized in Table S2.† It can be seen that different quantum dots all have different degrees of band gap reduction compared with the original wide-band gap TiO_2, which also proves that the research prospect of quantum dot sensitized solar cell itself has great potential and is worth exploring.

Firstly, PDOS of Ca_4O_4/TiO_2(001) is given as a representative of oxide quantum dots in Fig. 3a. Then, combined with relevant data in Table S2,† it can be seen that the whole adsorption system has four key orbitals, which include the highest occupied molecular orbital (HOMO) of the quantum dot, the valence band maximum (VBM) of the base material, the conduction band minimum (CBM) of the base material, and the lowest unoccupied molecular orbital (LUMO) of the quantum dot,

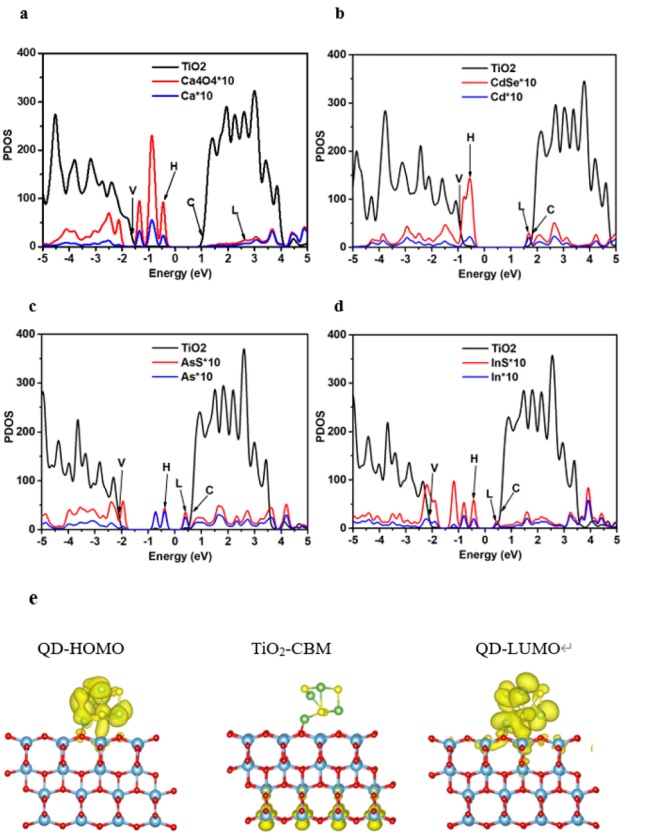

Fig. 3 PDOS of (a) Ca_4O_4/TiO_2(001), (b) Cd_4Se_4/TiO_2(001), (c) As_4S_4/TiO_2(001), (d) In_4S_4/TiO_2(001). (e) Charge isodensity diagrams for of As_4S_4/TiO_2(001). CaO is short for Ca_4O_4, and so on. To show the contrast more clearly, multiply the value of CaO by 10, like CaO × 10, and so on. 'V' and 'C' denote VBM and CBM of TiO_2(001); 'H' and 'L' denote HOMO and LUMO of QD.

respectively, from the lowest energy level to the highest energy level. In principle, this energy level arrangement is suitable for the application of quantum dot sensitized solar cells. The gap (CBM–HOMO) formed by $Ca_4O_4/TiO_2(001)$ adsorption system itself is only 1.54 eV, and the corresponding maximum wavelength of light is 807 nm, which has basically covered the visible spectrum. However, the LUMO orbital's energy level of Ca_4O_4 quantum dot is far from HOMO's, about 3.49 eV. The maximum absorption wavelength required for HOMO electrons to be excited to LUMO is only 356 nm, and this wavelength range almost completely avoids the whole visible spectrum (from about 400 nm to 800 nm). As a result, it is difficult for electrons of quantum dots to be excited under natural light conditions and transferred from LUMO of quantum dots to the conduction band of TiO_2. And as can be seen from the chart, other metal oxides of IIA group as quantum dots also have similar limitations with Ca_4O_4 (Fig. S2†).

As for the quantum dot structure of Cd_4O_4, Cd_4S_4 and Cd_4Se_4, it can be seen that there are similarities as well as particularity (Fig. S2† and 3b). The Cd_4O_4 reduced the gap of the adsorption system to the minimum of 1.50 eV, meaning that the maximum wavelength of excitation was 829 nm, which could cover the whole visible spectrum. However, it can be seen that HOMO and LUMO molecular orbitals of quantum dots are sandwiched between VBM and CBM of TiO_2, and the orbital energy level difference of LUMO–CBM reaches −1.1 eV, which is also the smallest energy difference of all materials in this calculation, while the energy difference of CBM–HOMO is 2.61 eV. This will result in an obvious physical phenomenon that in most cases the photoexcited electrons will be excited to the molecular orbital below CBM, thus making the transfer of electrons from the quantum dot to the conduction band impossible. The order of the VBM, HOMO, LUMO, CBM of $Cd_4S_4/TiO_2(001)$ and $Cd_4Se_4/TiO_2(001)$ on the energy levels is the same as that of $Cd_4O_4/TiO_2(001)$, but the difference of LUMO–CBM was small, which was −0.39 eV and −0.16 eV respectively, and the CBM–HOMO was 2.04 eV and 2.3 eV respectively (Fig. 3b and S2†). For this reason, the efficiency loss of photoexcited electron transfer of $Cd_4S_4/TiO_2(001)$ and $Cd_4Se_4/TiO_2(001)$ is smaller than that of $Cd_4O_4/TiO_2(001)$.

From the above two terms of light absorption and effective photoexcitation intensity, both $As_4S_4/TiO_2(001)$ and $In_4S_4/TiO_2(001)$ have a very good performance, so let's take a look at their PDOS in Fig. 3c and d. As can be seen from the figure, the gap of the $As_4S_4/TiO_2(001)$ and $In_4S_4/TiO_2(001)$ adsorption system is very small, 0.79 eV and 0.87 eV respectively, and the gap corresponds to the LUMO–HOMO of the quantum dot. And what we found is that for both of these adsorption systems, the HOMO and the LUMO are still between VBM and CBM, which is inconsistent with the ideal model. Fortunately, the gap itself is very small, and the LUMO–CBM energy level difference of $As_4S_4/TiO_2(001)$ is −0.24 eV, and the CBM–HOMO energy level difference is 1.03 eV; The LUMO–CBM energy level difference of $In_4S_4/TiO_2(001)$ was −0.16 eV, and the CBM–HOMO energy level difference was 1.03 eV. At the same time, we can also intuitively see that density of states of these materials including other sulfides above the molecular orbital of CBM is higher than that of oxides, which will also affect the power conversion efficiency (PCE). Fig. 3e shows the charge density diagram of each molecular orbital of $As_4S_4/TiO_2(001)$, revealing the possible charge transfer process. In summary, although $As_4S_4/TiO_2(001)$ and $In_4S_4/TiO_2(001)$ have PDOS that look similar to $Cd_4Se_4/TiO_2(001)$, they have smaller band gaps, resulting in greater fault tolerance and ultimately higher effective photoexcitation intensity.

For quantum-dot sensitized solar cells, the first step is that the quantum dots on the adsorption system absorb sunlight and generate photoexcited electrons. After the electrons are excited to the HOMO of the quantum dots, the second step is an ultra-fast process in which the electrons are transferred to TiO2's CBM and then enter the external circuit called photocurrent. Therefore, the proportion of photoexcited electrons transferred to TiO_2 conduction band is highly correlated with the energy conversion efficiency of quantum dot sensitized solar cells. In order to have a more suitable index to describe the efficiency of this key process, the concept of effective photoexcitation intensity is given, we use the following formulas to describe it.

$$A_{QD} = \int_{TiO_2-CBM}^{QD-HOMO+3\ eV} D_{QD}\, dE \quad (1)$$

$$A_{TiO_2} = \int_{CBM}^{CBE} D_{TiO_2}\, dE \quad (2)$$

$$I = \frac{A_{QD}}{A_{TiO_2}} \quad (3)$$

In eqn (1), A_{QD} is the integral of QD's density of states (DOS) from HOMO to HOMO+3 eV, where D_{QD} is the DOS, E is energy, 3 eV is the range of light absorption energy. In eqn (2), A_{TiO_2} is the integral of TiO_2's density of states over the whole range of the CB's first peak, where CBM is the conduction band minimum of the TiO_2, CBE is the lowest energy band. In eqn (3), I is effective photoexcitation intensity, which is calculated as the ratio of A_{QD} to A_{TiO_2}.

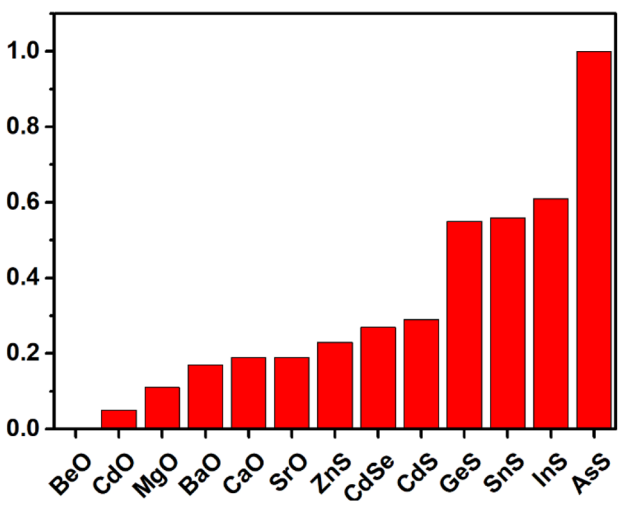

Fig. 4 Normalized effective photoexcitation intensity: BeO is short for $Be_4O_4/TiO_2(001)$, and so on.

By calculating the effective photoexcitation intensities of different QD/TiO_2(001) adsorption systems, we can intuitively see that the quantum dot sensitizers with the best performance in the electron transfer process, and the relevant data are given in Table S1 in the ESI.† It can be seen from the table that As_4S_4/TiO_2(001) has the maximum effective photoexcitation intensity, which is about 1.6 times of the effective photoexcitation intensity of In_4S_4/TiO_2(001). Let's normalize effective photoexcitation intensity value of As_4S_4/TiO_2(001), then the histogram of all normalized effective photoexcitation intensity is given (Fig. 4). Both sulfides and selenides performed better than oxides under the condition of normalized effective photoexcitation intensity. Considering from two aspects of light absorption and effective photoexcitation intensity, the possibility of the oxide mentioned in this study as a kind of excellent quantum dot sensitizer has almost disappeared. It's important to focus on sulfides and selenides, to see which compounds have good results in both photo absorption and effective photoexcitation. First of all, it was revealed that the As_4S_4/TiO_2(001) adsorption system performed best in both aspects and was much higher than the second place. Next, the normalized effective photoexcitation intensity of In_4S_4/TiO_2(001), Sn_4S_4/TiO_2(001) and Ge_4S_4/TiO_2(001) was 0.61, 0.56 and 0.55, respectively, which could be regarded as Performance is similar, coincidentally, the light absorption performance of these adsorption systems also occupies the top and middle position in Fig. 2d. At the same time, the effective photoexcitation intensity of oxide-QD/TiO_2 adsorption system with poor light absorption performance also had the worst performance. In fact, we can realize that there is a correlation between the light absorption effect and the effective photoexcitation intensity of the adsorption system. The reason for this correlation is that the band gap of the whole adsorption system is reduced by quantum dot sensitization, more electrons can be excited to LUMO in the Narrow band gap QD/TiO_2(001) adsorption system, therefore, this will improve both the light absorption efficiency and the electron transfer probability. A special kind of adsorption system is Cd_4Se_4/TiO_2(001), it has the second light absorption capacity, but its normalized effective photoexcitation intensity value is only 0.27, even lower than the Cd_4S_4/TiO_2(001)'s value of 0.29. There are two reasons for this phenomenon. One is that Cd_4Se_4 itself has a wide band gap, and the other is that the LUMO of Cd_4Se_4 is located below the energy level of TiO_2's CBM, so that a large number of excited electrons cannot be transferred to the conduction band.

3.4 Adsorption strength

As the photoanode of quantum-dot sensitized battery, the adsorption stability of QD/TiO_2(001) composite structure is very important. We need to discuss how the quantum-dot adsorbed on the surface of TiO2(001). Therefore, the energy calculation of quantum dots adsorbed on the surface of TiO_2 porous film was constructed. At first, the structure of $4 \times 2 \times 2TiO_2$(001) adsorbed without quantum dots was optimized and the energy was calculated. Next, the structure of $2 \times 2 \times 2$ quantum dots of IIA, Cd_4O_4, Cd_4S_4, Cd_4Se_4 and some other sulfides was optimized and the energy was calculated. Then, each quantum dot was adsorbed on the surface of $4 \times 2 \times 2TiO_2$(001) for structural optimization, and the adsorption stability between it and the structure of the substrate was observed, and the total energy was obtained, so we were able to come up with a standard for determining the stability of the structure: adsorption energy (E_{ads}).

$$E_{ads} = (E_{QD/TiO_2} - E_{TiO_2} - E_{QD}) \quad (4)$$

where E_{QD/TiO_2} is the energy of QD/TiO_2 adsorption system, E_{TiO_2} is the energy of $4 \times 2 \times 2$-TiO_2, E_{QD} is the energy of QD.

As shown in Fig. 5, the IIA group oxide-QD/TiO_2 composite system has high stability, which is due to the fact that both the quantum dot and the base are metal oxides. In the quantum dot, the metal and the oxygen on the base surface form a covalent bond, and the Ti on the base surface also forms a covalent bond with the oxygen of the quantum dot. The adsorption of the Ca_4O_4/TiO_2(001) composite system was the most stable, and the additional reasons were the proper size cube structure of Ca_4O_4 and the regular arrangement of atoms on the surface of TiO_2, leading to the fact that the lower part of the cube of metal oxides could fit into the square composed of atoms on the surface of TiO_2. According to the NIST Atomic Spectra Database, Potential of 2 electrons ionized from Ca is 11.87 eV, while the adsorption energy of Ca_4O_4/TiO_2(001) is −12.17 eV.[43]

As shown in the Ca_4O_4/TiO_2(001) composite structure in Fig. S1,† it can be seen that one O of Ca_4O_4 is directly opposite one Ti on the surface of TiO_2, and its distance is 1.91 Å, and it's actually going to be the closest oxygen around this corresponding Ti atom, while in TiO_2 structure, the minimum distance between O bonding with Ti is 1.97 Å, and the distance between other oxygen atoms is 1.99 Å, 2.17 Å, 2.20 Å and 2.23 Å, respectively. Ca in Ca_4O_4 is directly opposite the middle point of the side length of the square on the surface of TiO_2. Both side points are occupied by O. The distance between Ca and each O is 2.35 Å and 2.34 Å respectively, which is also close to the Ca–O bond length of Ca_4O_4. As the structural bond lengths of other metal oxides do not fit the surface morphology of TiO_2 so well

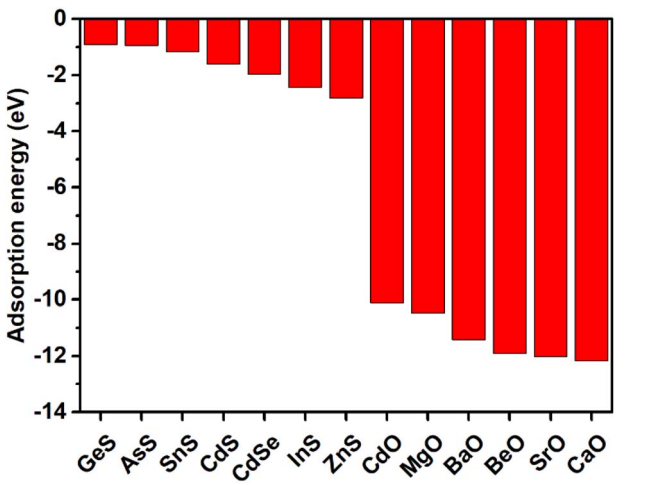

Fig. 5 Adsorption energy of QD/TiO_2(001): GeS is short for Ge_4S_4/TiO_2(001), and so on.

like Ca_4O_4, they will change their own morphology and the surface morphology of TiO_2 to reach the most stable adsorption state.

Since Cd_4S_4 and Cd_4Se_4 are effective quantum dot solar cell materials that have been experimentally verified, the stability of $(MA)_4$ quantum dots of Cd element compound on the surface of TiO_2 is also worthy of our attention. As can be seen from Fig. 5, the adsorption energy of Cd_4S_4, Cd_4Se_4 and Cd_4O_4 are −0.40 eV, −0.49 eV and −2.53 eV respectively. For the same reason as Ca_4O_4, Cd_4O_4 has higher adsorption energy compared with Cd_4S_4 and Cd_4Se_4, and it can be seen from its structure that its most stable adsorption mode is also similar to Ca_4O_4 (Fig. S1†). Different from Cd_4O_4 and Cd_4S_4, Cd_4Se_4 adsorbed on the surface of TiO_2 at an inclined Angle, as shown in Fig. 1b, A Cd at the bottom of Cd_4Se_4 quantum dot was closer to the surface of TiO_2, and also in the center of a square edge on the surface, Oxygen atoms occupied by two nearby points were 2.23 Å and 2.24 Å far from Cd, respectively. The other Cd atom is far away from the surface of the film, while the distance between the two Se atoms at the bottom of the quantum dot is 2.73 Å and 2.74 Å respectively, which changes the structure of the quantum dot itself and also makes it tilt. Thus, it can be concluded that the adsorption energy of quantum dots on the surface of TiO_2 is mainly contributed by the O–Ti bond, and neither S–Ti nor Se–Ti has high bond energies.

The sulfide exhibited good performance in both light absorption and effective photoexcitation intensity, but had weak adsorption stability. For the $As_4S_4/TiO_2(001)$ adsorption system, the adsorption energy is −0.94 eV. As_4S_4 slightly deformed and tilt, looks like Cd_4Se_4. One As of QD is closer to TiO_2 surface, with the nearest As–O bond length of 1.89 Å. Other atoms are further away from the surface, the overall adsorption is still relatively weak, and should be mainly contributed by the As–O bond energy. The adsorption stabilities of sulfides are slightly weaker, which will indeed weaken their advantage as a kind of quantum dots sensitizers, but at the same time, its adsorption energy remains at a reasonable level, which it is still worth applying it to the quantum dot sensitized solar cell.

3.5 M_4A_3B and $M_4A_2B_2$ QD/TiO_2 heterojunction

From the $(MA)_4/TiO_2$ heterojunction results, it can be seen that oxygen atoms have a positive effect on increasing adsorption stability. Therefore, we decided to replace $1 \sim 2$ S or Se atoms in As_4S_4, In_4S_4 and Cd_4Se_4, which had the best performance in light absorption and PCE, with O atoms. As shown in Fig. 6a, two sulfur atoms in the quantum dots adsorbed on the surface of the base material were replaced with oxygen atoms, is $As_4S_2O_2/TiO_2(001)$. And in Fig. 6b, $As_4S_3O/TiO_2(001)$ means only one sulfur atom was replaced with oxygen atom. Because oxygen atoms have stronger adsorption stability than sulfur atoms on the surface of titanium dioxide, original structure of the quantum dots has been completely torn apart, So $As_4S_2O_2/TiO_2(001)$ can be classified as mixed adsorption type. Fig. S1† Shows several other geometries of the optimized adsorption system include $Cd_4Se_2O_2/TiO_2(001)$, $Cd_4Se_3O/TiO_2(001)$,

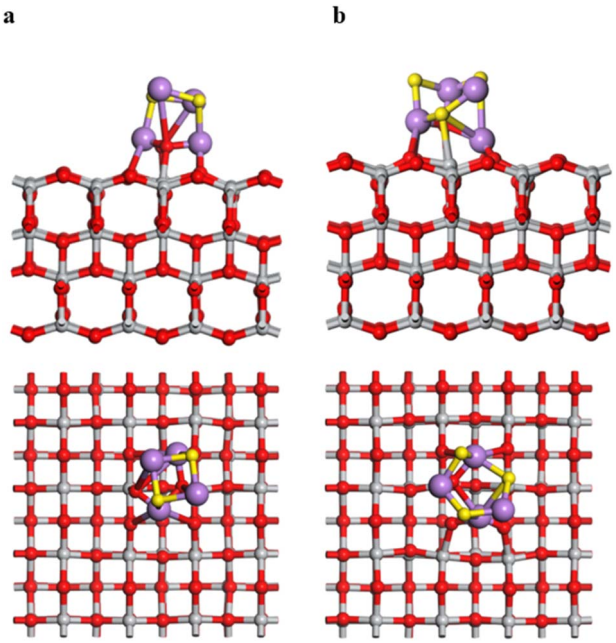

Fig. 6 The geometry of the optimized adsorption system (a) $As_4S_2O_2/TiO_2(001)$, (b) $As_4S_3O/TiO_2(001)$.

$In_4S_2O_2/TiO_2$ (001) and In_4S_3O/TiO_2 (001). They can be classified as lattice symmetry adsorption type, because the original quantum dot structure fit the $TiO_2(001)$ surface lattice well and the optimization deformation is slightly smaller.

The same three criteria including adsorption stability, light absorption intensity and effective photoexcitation intensity will be used to compare Hetero-chalcogenide atoms QD/TiO_2 (001) and chalcogenide atoms QD/TiO_2 (001). In Fig. 7a, With the increase of the number of O atoms replacing S atoms, the adsorption strength of all quantum dot systems increased significantly. Although the adsorption energy of $As_4S_2O_2/TiO_2(001)$ increases twice as much as that of $As_4S_4/TiO_2(001)$, it is still only −2.5 eV. The adsorption energy of $In_4S_2O_2/TiO_2(001)$ and $Cd_4Se_2O_2/TiO_2(001)$ are −5.16 eV and −5.23 eV, respectively. It can be seen that the quantum dot system replaced with two oxygen atoms has the adsorption strength close to that of the oxide quantum dot system. Next, the light absorption intensity was investigated to see whether the light absorption performance was reduced due to the addition of oxygen atoms. As shown in Fig. 7b, As expected, the light absorption performance did deteriorate with the addition of oxygen atoms, but it was still much better than the light absorption performance of oxide quantum dots. The abnormal values of $As_4S_2O_2/TiO_2(001)$ and $As_4S_3O/TiO_2(001)$ may be due to the large difference between the structure of As_4S_4 and the lattice on the surface of titanium dioxide, so the structure of the quantum dot itself becomes very irregular after the addition of one or two oxygen atoms. Although the light absorption intensity of the quantum dot adsorption system is important, it cannot be regarded as an ideal material if it cannot effectively excite the electron transition. In Fig. 7c, normalized effective photoexcitation intensity of QD//$TiO_2(001)$ be counted out. As for As_4S_4 quantum dots, with

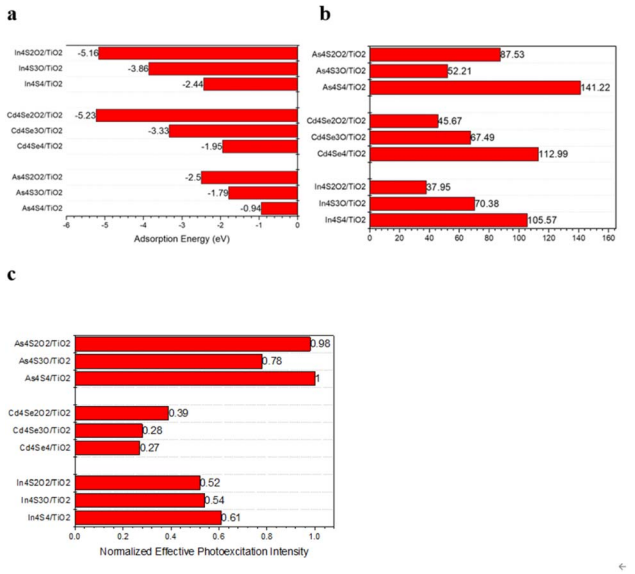

Fig. 7 Photoelectric performance comparison: (a) adsorption energy (b) the area of each light absorption spectrum in the visible band of 400–800 nm. (c) Normalized effective photoexcitation intensity.

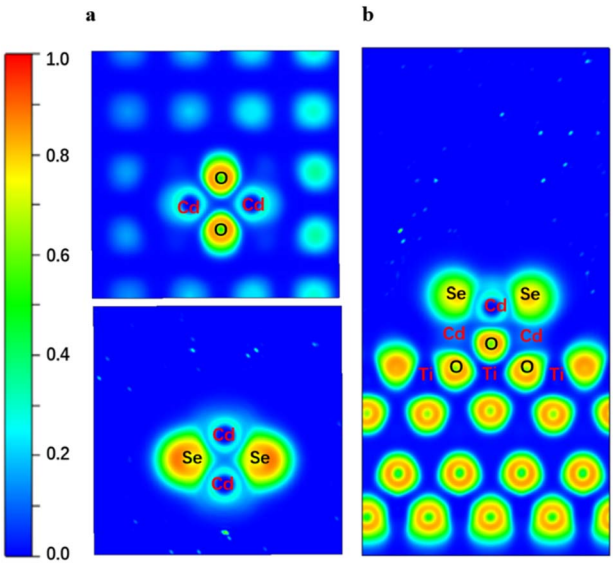

Fig. 8 ELF plots of $Cd_4Se_2O_2/TiO_2$, projected on the: (a) (001) plane, (b) (100) plane.

the substitution of O atom for S atom, its normalized effective photoexcitation intensity does not decrease significantly, even the values of $As_4S_2O_2/TiO_2(001)$ and $As_4S_4/TiO_2(001)$ are basically the same. More interesting, normalized effective photoexcitation intensity of $Cd_4Se_2O_2/TiO_2(001)$ is 0.39, while that of $Cd_4Se_4/TiO_2(001)$ is 0.27. This phenomenon indicates that although the effective photoexcitation intensity of Cd_4O_4 quantum dots is lower than that of CdSe, when Se atoms are replaced by some oxygen atoms, the effective excusable light intensity of the quantum dot system is higher than both of them. $In_4S_2O_2/TiO_2(001)$ has a good performance in the two indexes of adsorption stability and light absorption intensity, and its normalized effective photoexcitation intensity does not decay greatly with the addition of oxygen atoms.

To better analyse the chemical bonds between the quantum dots and the surface, in Fig. 8, the electron localization function (ELF) is used to describe the chemical bonds of QD_S and surfaces. As for $Cd_4Se_2O_2$ in $Cd_4Se_2O_2/TiO_2(001)$, Fig. 8a shows the electrons are localized to the O and Se atoms, which means that Cd forms an ionic bond with the Se, O atoms. The bond length of Cd–O is 2.46 Å, and the bond length of Cd–Se is 2.67 Å. From Fig. 8b, the electrons on the surface of $TiO_2(001)$ are also localized to O atoms, so the Ti on the surface forms an ionic bond with the O atom of the quantum dot, which the band length of Ti–O is 1.93 Å, while the Ti–O band length of surface is 1.98 Å. And the Cd atom of the quantum dot forms an ionic bond with the O atom on the surface, which the band length of Cd–O is 2.28 Å. It can be seen that the Ti–O ionic bonds make a major contribution for the structural stability of the adsorption system. The bonding pattern between the quantum dots and the surface in $In_4S_2O_2/TiO_2$ is similar to that in $Cd_4Se_2O_2/TiO_2(001)$ and has been shown in Fig. S3.† In Fig. S3(a),† Electrons are localized on O atoms, and an ionic bond is formed between O and In atom with a bond length of 2.25 Å. The bonds between the quantum dots and the surface are shown in Fig. S3(b),† where electrons are localized to the oxygen atoms in the QD_S and on the surface. The In atom forms an ionic bond with the surface O atom, and the bond length is 2.2 Å. The O atom in the quantum dot also forms an ionic bond with the Ti atom on the surface, and the bond length is 1.92 Å, which means that the Ti–O bond is strong. It can be seen from the above that the bond energy of Ti–O is the main contribution to the adsorption stability of the quantum dot heterojunction.

The ELF calculation results of $As_4S_2O_2/TiO_2$ are slightly different and are shown in Fig. S4.† As for $As_4S_2O_2$, Electrons are distributed on each atom, and there is an electron distribution between each atom, with ELF = 0.5, which means that As–O and As–S are covalent bonds, as shown in Fig. S4(a).† Due to the irregular structure, As–O band lengths are 1.89 Å, 1.91 Å and 1.92 Å, and there is an As atom and an O atom that are not bonded to each other, and the distance between them is 3.23 Å. As–S bonds are the same length, 2.3 Å, because it is not close to the surface, there is less deformation. The bonding between the quantum dot and the surface is shown in Fig. S4(b).† It can be seen that an As in the quantum dot forms a covalent bond with O on the surface, and the bond length is 1.95 Å, but the other As atom in the quantum dot is far away from the surface, and the distance between it and the oxygen atom on the surface is 3.1 Å. The two O atoms in the quantum dot form ionic bonds with the two Ti atoms on the surface, with bond lengths of 2.05 Å and 2.25 Å, respectively. It can be seen that the bond length between $As_4S_2O_2$ and the surface is longer, and one of the As atoms is far away from the surface, which means that the adsorption stability of $As_4S_2O_2/TiO_2$ is worse than that of $Cd_4Se_2O_2/TiO_2(001)$. Our adsorption stability calculation data also meet this expectation. ELF calculation results illustrate the bonding

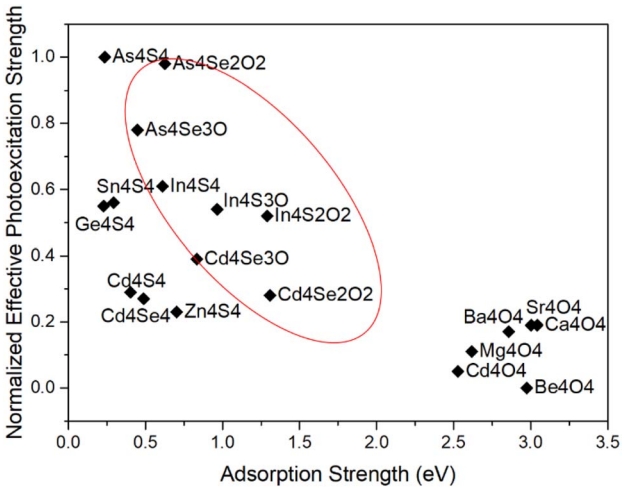

Fig. 9 Coordinates of QD/TiO_2(001) adsorption system, the horizontal axis is adsorption energy, and the vertical axis is normalized effective photoexcitation intensity.

between the quantum dots and the surface in detail, and further verify that the O atoms in the quantum dots are easy to bond with the surface, which is conducive to the stability of the adsorption system.

Finally, we plot the coordinates of each adsorption system in Fig. 9, where the horizontal axis is unit adsorption energy and the vertical axis is normalized effective photoexcitation intensity. The materials in the red circle of Fig. 6 have the advantages of both adsorption stability and high light absorption efficiency.

Compared with the CdO/CdSe quantum dot sensitized solar cell in previous experiments, Quantum dots with mixed elements have obvious advantages. $Cd_4Se_2O_2$ improves the position of the conduction band, ultimately improves the electron injection rate and the corresponding photoelectric conversion efficiency. Cd_4S_3O not only reduces the band gap but also improves the adsorption stability of the material. This can be seen as an improvement over conventional quantum dots. At the same time, we have found A group of quantum dots that perform better in theoretical calculations, such as $As_4S_2O_2$ and $In_4S_2O_2$. These new materials have a larger light absorption range and effective excited light intensity while maintaining high stability of the material. Therefore, there is reason to believe that they have better application prospects in experimental species.

This picture can inspire us to find more materials to fill suitable candidate areas of materials, such as the construction of novel sensitizers with advantageous properties of sulfides and oxides.

4. Conclusion

In summary, we compared a series of sulfides, selenides and oxide quantum dots with the same structure as sensitizers to form an adsorption system with TiO_2. We mainly took the light absorption and effective photoexcitation intensity of the QD/TiO_2(001) adsorption system as the assessment indicators, and finally referred to the adsorption stability of each system. Eventually, hetero-chalcogenide atoms QD shows good adsorption stability, light absorption intensity and effective photoexcitation intensity. In particular, it provides guidance for finding new configurations of quantum dots, which can meet these criteria at the same time. More importantly, we hope to provide a candidate range of quantum dot sensitizer materials, so as to stimulate the search for new materials with common characteristics.

Conflicts of interest

There are no conflicts to declare.

Acknowledgements

The authors gratefully acknowledge the funding from the Beijing Computational Science Research Center and the computational resources from TH2-JK supercomputer at the Beijing Computational Science Research Center.

Notes and references

1 D. M. Chapin, C. S. Fuller and G. L. Pearson, *J. Appl. Phys.*, 1954, **25**, 676–677.
2 W. Shokley and H. J. Queisser, *J. Appl. Phys.*, 1961, **32**, 510–519.
3 S. Rühle, *Sol. Energy*, 2016, **130**, 139–147.
4 J. B. Sambur, T. Novet and B. A. Parkinson, *Science*, 2010, **330**, 63–66.
5 A. P. Alivisatos, *Science*, 1996, **271**, 933–937.
6 P. V. Kamat, *J. Phys. Chem. Lett.*, 2013, **4**, 908–918.
7 J. Tian and G. Cao, *Nano Rev.*, 2013, **4**, 22578.
8 B. O'Regan and M. Gratzel, *Nature*, 1991, **353**, 737–740.
9 Z. Pan, H. Rao, I. Mora-Sero, J. Bisquert and X. Zhong, *Chem. Soc. Rev.*, 2018, **47**, 7659–7702.
10 A. Hagfeldt, G. Boschloo, L. C. Sun, L. Kloo and H. Pettersson, *Chem. Rev.*, 2010, **110**, 6595–6663.
11 G. Saranya, C. Y. Yam, S. Gao and M. Chen, *J. Phys. Chem. C*, 2018, **122**, 23280–23287.
12 P. G. Johansson, J. G. Rowley, A. Taheri and G. J. Meyer, *Langmuir*, 2011, **27**, 14522–14531.
13 G. Hodes, *J. Phys. Chem. C*, 2008, **112**, 17778–17787.
14 I. Robel, V. Subramanian, M. Kuno and P. V. Kamat, *J. Am. Chem. Soc.*, 2006, **128**, 2385–2393.
15 A. J. Nozik, *Physica E*, 2002, **14**, 115–120.
16 Y. L. Lee and Y. S. Lo, *Adv. Funct. Mater.*, 2009, **19**, 604–609.
17 B. Yuan, Q. Gao, X. Zhang, *et al*, *Electrochim. Acta*, 2018, **1**, 50–88.
18 Z. Pan, L. Yue, H. Rao, *et al.*, *Adv. Mater.*, 2019, **31**, 1903696.
19 A. Kongkanand, K. Tvrdy, K. Takechi, M. Kuno and P. V. Kamat, *J. Am. Chem. Soc.*, 2008, **130**, 4007–4015.
20 A. J. Nozik, M. C. Beard, J. M. Luther, M. Law, R. J. Ellingson and J. C. Johnson, *Chem. Rev.*, 2010, **110**, 6873–6890.
21 J. B. Sambur, T. Novet and B. A. Parkinson, *Science*, 2010, **330**, 63–66.

22 O. E. Semonin, J. M. Luther, S. Choi, H.-Y. Chen, J. Gao, A. J. Nozik and M. C. Beard, *Science*, 2011, **334**, 1530–1533.
23 T. Su, Z. Qin, H. Ji, Y. Jiang and G. Huang, *Environ. Chem. Lett.*, 2015, **14**, 99–112.
24 S. N. F. Moridon, K. Arifin, R. M. Yunus, L. J. Minggu and M. B. Kassim, *Ceram. Int.*, 2022, **48**, 5892–5907.
25 N. K. Bharti and B. Modak, *J. Phys. Chem. C*, 2022, **126**(36), 15080–15093.
26 F. Khodam, A. R. A. Ghadim and S. Aber, *Sol. Energy*, 2019, **181**, 325–332.
27 D. Liu, J. Liu, *et al*, *Phys. E*, 2020, **115**, 113669.
28 K. Lv, C. Shi, C. Ma, *et al*, *J. Nanopart. Res.*, 2019, **21**, 2.
29 Q. Zhang, X. Guo, X. Huang, *et al.*, *Phys. Chem. Chem. Phys.*, 2011, **13**, 4659–4667.
30 J. Du, Z. Du and J. S. Hu, *J.Am.Chem.Soc*, 2016, **138**, 4201–4209.
31 S. Jiao, J. Du, Z. Du, D. Long, W. Jiang, Z. Pan, Y. Li and X. Zhong, *J. Phys. Chem. Lett.*, 2017, **8**, 559–564.
32 L. Liu and A. Corma, *Chem. Rev.*, 2018, **118**, 4981–5079.
33 C. Papatriantafyllopoulou, E. E. Moushi, G. Christou and A. J. Tasiopoulos, *Chem. Soc. Rev.*, 2016, **45**, 1597–1628.
34 S. G. Kwon and T. Hyeon, *Acc. Chem. Res.*, 2008, **41**, 1696–1709.
35 E. Martinez-Ferrero, I. M. Sero, J. Albero, S. Gimenez, J. Bisquert and E. Palomares, *Phys. Chem. Chem. Phys.*, 2010, **12**, 2819–2821.
36 H. Zhang, K. Cheng, Y. M. Hou, Z. Fang, Z. X. Pan, W. J. Wu, J. L. Hua and X. H. Zhong, *Chem. Commun.*, 2012, **48**, 11235–11237.
37 M. Chen, A. R. Felmy and D. A. Dixon, *J. Phys. Chem. A*, 2014, **118**, 3136–3146.
38 M. Chen, K. S. Thanthiriwatte and D. A. Dixon, *J. Phys. Chem. C*, 2017, **121**, 23025–23038.
39 S. G. Kwon and T. Hyeon, *Acc. Chem. Res.*, 2008, **41**, 1696–1709.
40 E. Martinez-Ferrero, I. M. Sero, J. Albero, S. Gimenez, J. Bisquert and E. Palomares, *Phys. Chem. Chem. Phys.*, 2010, **12**, 2819–2821.
41 H. Zhang, K. Cheng, Y. M. Hou, Z. Fang, Z. X. Pan, W. J. Wu, J. L. Hua and X. H. Zhong, *Chem. Commun.*, 2012, **48**, 11235–11237.
42 M. Chen, A. R. Felmy and D. A. Dixon, *J. Phys. Chem. A*, 2014, **118**, 3136–3146.
43 A. Kramida and J. Res, *Natl. Inst. Stand. Technol.*, 2013, **118**, 52–104.